Structure

Binding of steroid substrates reveals the key to the productive transition of the cytochrome P450 OleP

Graphical abstract

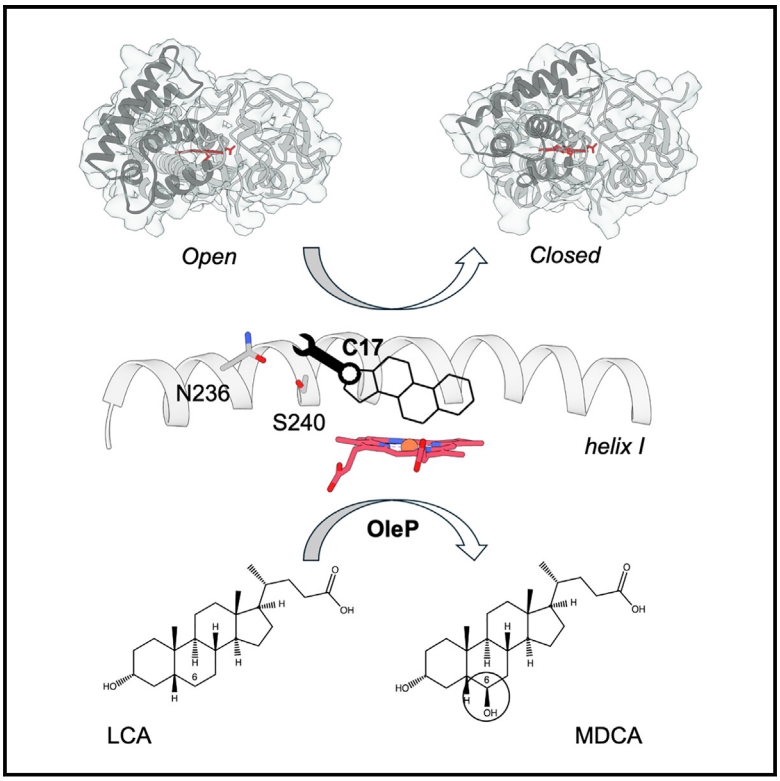

Highlights

- Crystal structures of OleP in complex with steroids were determined
- Binding to lithocholic acid efficiently activates the closure of the OleP active site
- The C17 substituent in steroids affects the selectivity of the OleP reaction

Authors

Antonella Costanzo, Francesca Fata, Ida Freda, ..., Beatrice Vallone, Carmelinda Savino, Linda Celeste Montemiglio

Correspondence

beatrice.vallone@uniroma1.it (B.V.), carmelinda.savino@cnr.it (C.S.), lindaceleste.montemiglio@cnr.it (L.C.M.)

In brief

OleP is a cytochrome P450 epoxygenase involved in oleandomycin biosynthesis, and it also hydroxylates lithocholic acid and testosterone. By combining X-ray crystallography, binding assays, and molecular dynamics simulations, Costanzo et al. found that the C17 substituent group of steroids influences the structural transition and reaction selectivity of OleP.

Costanzo et al., 2024, Structure *32*, 1–12
September 5, 2024
https://doi.org/10.1016/j.str.2024.06.005

CellPress

Structure

CellPress
OPEN ACCESS

Article

Binding of steroid substrates reveals the key to the productive transition of the cytochrome P450 OleP

Antonella Costanzo,[1,2,9] Francesca Fata,[3,9] Ida Freda,[1,6,9] Maria Laura De Sciscio,[4] Elena Gugole,[3] Giovanni Bulfaro,[1,2] Matteo Di Renzo,[1,7] Luca Barbizzi,[1,8] Cécile Exertier,[3] Giacomo Parisi,[5] Marco D'Abramo,[4] Beatrice Vallone,[1,3,*] Carmelinda Savino,[3,*] and Linda Celeste Montemiglio[3,10,*]

[1]Department of Biochemical Sciences "Alessandro Rossi Fanelli", Sapienza, University of Rome, P. le Aldo Moro, 5, 00185 Rome, Italy
[2]Takis Biotech, Via di Castel Romano 100, 00128 Rome, Italy
[3]Institute of Molecular Biology and Pathology c/o Department of Biochemical Sciences "Alessandro Rossi Fanelli", Sapienza, University of Rome, National Research Council, P.le Aldo Moro, 5, 00185 Rome, Italy
[4]Department of Chemistry, University of Rome, Sapienza, P.le A. Moro 5, 00185 Rome, Italy
[5]Department of Basic and Applied Sciences for Engineering (SBAI), Sapienza, University of Rome, Via Antonio Scarpa, 16, 00161 Rome, Italy
[6]Present address: Department of Molecular Medicine, University of Pavia, Via Ferrata 9, 27100, Pavia, Italy
[7]Present address: Department of Management, Sapienza, University of Rome, Via del Castro Laurenziano, 9, 00181, Rome, Italy
[8]Present address: Thermofisher Scientific, Via Morolense, 5, 03013, Ferentino (FR), Italy
[9]These authors are contributed equally
[10]Lead contact
*Correspondence: beatrice.vallone@uniroma1.it (B.V.), carmelinda.savino@cnr.it (C.S.), lindaceleste.montemiglio@cnr.it (L.C.M.)
https://doi.org/10.1016/j.str.2024.06.005

SUMMARY

OleP is a bacterial cytochrome P450 involved in oleandomycin biosynthesis as it catalyzes regioselective epoxidation on macrolide intermediates. OleP has recently been reported to convert lithocholic acid (LCA) into murideoxycholic acid through a highly regioselective reaction and to unspecifically hydroxylate testosterone (TES). Since LCA and TES mainly differ by the substituent group at the C17, here we used X-ray crystallography, equilibrium binding assays, and molecular dynamics simulations to investigate the molecular basis of the diverse reactivity observed with the two steroids. We found that the differences in the structure of TES and LCA affect the capability of these molecules to directly form hydrogen bonds with N-terminal residues of OleP internal helix I. The establishment of these contacts, by promoting the bending of helix I, fosters an efficient trigger of the open-to-closed structural transition that occurs upon substrate binding to OleP and contributes to the selectivity of the subsequent monooxygenation reaction.

INTRODUCTION

Steroid-based drugs hold paramount significance in medicine and pharmaceutical industry. Serving diverse physiological effects, these molecules are extensively employed for the treatment of a wide spectrum of disorders such as inflammation, cancers, allergies, and contraception.[1,2] Differences in the substituent groups at the C17 position and in the hydroxylation pattern of the core drive their biological activity, varying their pharmacokinetic and pharmacodynamic profiles.[3] Hydroxylation is considered the most relevant functionalization of a steroidal compound: the increased polarity of the resulting molecule is associated to enhanced biological activity and lower toxicity. Nevertheless, the introduction of hydroxyl groups on the nonactivated carbons of the steroidal nucleus poses a considerable challenge when employing traditional synthetic approaches since it requires a precise control of the regioselectivity. Among the alternative strategies under investigation, the use of cytochrome P450s (P450s) as biocatalysts emerges prominently.[4–7]

P450s are heme-containing enzymes that play critical roles in several metabolic pathways across organisms, ranging from drug metabolism to the synthesis of endogenous compounds. One remarkable aspect of P450s lies in their intrinsic ability to interact with a multitude of substrates. This biotechnologically significant trait paves the way for the strategic utilization of these enzymes to selectively introduce alternative functions on intricate molecules.[8] Bacterial P450s are generally preferred for such applications over their eukaryotic counterparts, due to the higher stability and expression levels together with easier manipulation and engineering procedures which are associated to lower production costs.[8,9]

The bacterial P450 OleP is one of the tailoring enzymes involved in the biosynthesis of the macrolide antibiotic oleandomycin.[10–12] It is capable of catalyzing the rare reaction of epoxidation of an unreactive C–C bond, possibly passing through an

Please cite this article in press as: Costanzo et al., Binding of steroid substrates reveals the key to the productive transition of the cytochrome P450 OleP, Structure (2024), https://doi.org/10.1016/j.str.2024.06.005

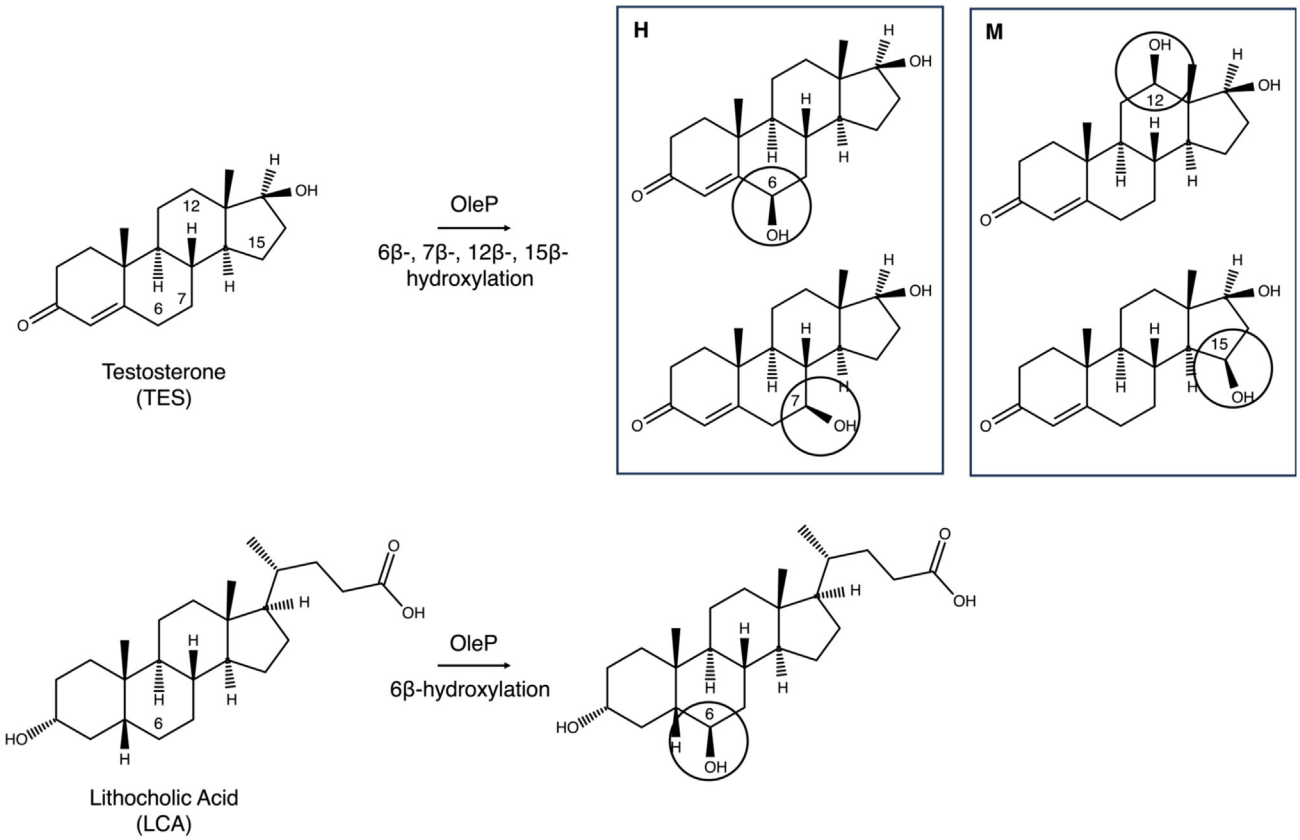

Figure 1. Scheme of the hydroxylation reaction of TES and LCA performed by OleP

Black boxes divide the TES hydroxylated products into two groups: those with a conversion rate exceeding 10% (H) and those with a conversion rate ranging between 10% and 5% (M).[18]

olefinic intermediate which is produced by OleP itself.[13] The unique chemistry carried out by this enzyme renders it particularly interesting for biotechnological applications as a biocatalyst.[14] In this perspective, another attractive feature of the enzymatic activity of OleP is its intrinsic substrate promiscuity as the P450 can react on multiple intermediates of the oleandomycin biosynthetic pathway, namely 8.8a-deoxyoleandolide (DEO) and L-olivosyl-8.8a-deoxyoleandolide (L-*O*-DEO).[13] Based on crystallographic data and in silico docking analysis, we proposed L-O-DEO as the preferential substrate.[15] This latter intermediate carries all the structural elements, i.e., a 14-membered macrolactone ring and one L-olivosyl sugar at the C3 position, to fully occupy the active site of OleP. Indeed, only the presence of a sugar moiety enables L-O-DEO, placed at the distal site, to extend over a cavity that is occupied by solvent molecules when the sole DEO aglycone is bound.[15,16] For this reason, we referred to this cavity as the solvent cavity. The computational docking of L-O-DEO in the OleP active site showed that within the solvent cavity, the L-olivosyl moiety of L-O-DEO forms direct hydrogen bonds with N-terminal residues of the helix I, namely N236 and S240.[15] We proposed that these interactions may provide the major contribution to the open-to-closed structural transition of OleP induced by substrate binding, the closed conformation being the catalytically competent state.[15–17]

The natural versatility of this enzyme has been further explored by testing its activity on alternative substrates. More specifically, OleP has been reported to hydroxylate steroidal compounds, such as testosterone (TES) and lithocholic acid (LCA).[18,19] These molecules mainly differ by the substituent group at the C17, that is a hydroxyl function in the case of TES and a long chain of pentanoic acid in the LCA structure (Figure 1). This difference has an impact on the reactivity of OleP: while the reaction on TES is unspecific as it yields a mixture of 6β-, 7β-, 12β-, and 15β-hydroxylated derivatives,[18] the reaction against LCA is highly selective as it produces murideoxycholic acid (MCDA) as the sole 6β-hydroxylated product (Figure 1).[19]

Unveiling the molecular basis driving OleP regio- and stereoselectivity of steroid hydroxylation would pave the way toward a potential use of OleP as a biotechnological tool to produce valuable steroid-based agents endowed with neuroprotective and anti-inflammatory activities.

With the aim to understand how the binding of different substrates drives the selectivity of the OleP reaction, we solved the structures of the complexes formed with LCA and TES by X-ray crystallography and we performed molecular dynamics (MD) simulations and equilibrium binding experiments to characterize the binding properties.

Our structural data indicate that TES only partially occupies the active site of OleP, filling the heme distal pocket. Conversely,

Please cite this article in press as: Costanzo et al., Binding of steroid substrates reveals the key to the productive transition of the cytochrome P450 OleP, Structure (2024), https://doi.org/10.1016/j.str.2024.06.005

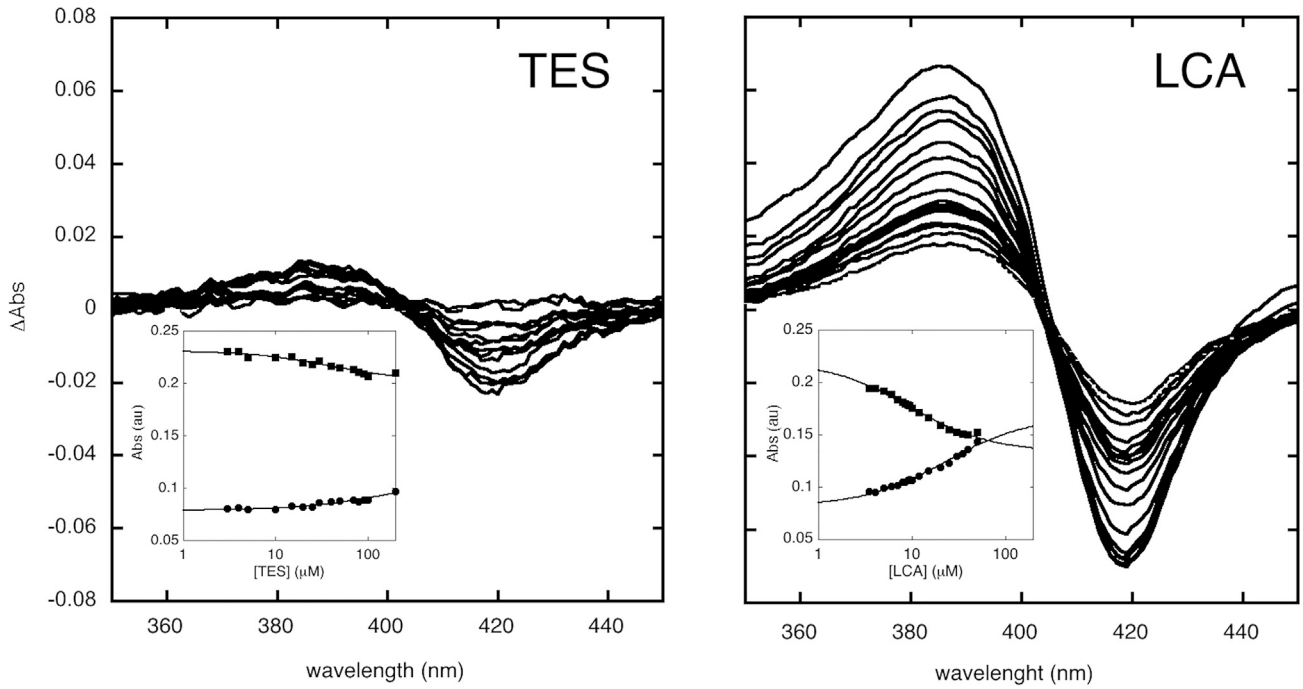

Figure 2. Spectrophotometric equilibrium binding experiments of OleP with TES and LCA at 298 K

Representative difference spectra obtained upon titration of OleP with the steroid substrates are shown. Data in the insets report the absorbance intensities of OleP, used at a constant concentration, monitored at 417 nm (full squares) and at 388 nm (full dots) as a function of the logarithm of total TES and LCA concentration in 50 mM HEPES, and 200 mM NaCl, pH 7.5. Solid lines are the best fit to a hyperbolic function. See also Table S1.

LCA is fully embedded in the active site, with the steroid unit occupying the distal site and the pentanoic acid chain filling the solvent cavity, where it establishes direct hydrogen bonds with N236 and S240. The simultaneous docking to both the distal site and the solvent cavity of the OleP active site allows LCA to arrange in a unique and stable pose, as indicated by MD simulations. In this position, the C6 is β-oriented toward the heme iron and placed at an optimal distance for the hydroxylation reaction.

The observation of a higher accumulation of the high spin closed conformer in the presence of LCA with respect to TES in solution indicates that the formation of these contacts enables an efficient trigger of the open-to-closed conformational change in OleP.

RESULTS AND DISCUSSION

Steroid binding to the P450 OleP

The binding properties of OleP toward TES and LCA were investigated by titrating the P450 against the two steroidal compounds at 298 K. The variation of the UV-visible absorption spectrum of the heme iron was monitored at different ligand concentrations.[20,21] Upon binding to TES or LCA, OleP exhibits a type I spectral shift of the Soret band, typically observed with P450 substrates, with a peak at 417 nm and a through at 388 nm (Figure 2).

The equilibrium binding transition of OleP to both steroid compounds is consistent with a simple hyperbolic function at all recorded wavelengths, which is indicative of a single binding event, returning apparent K_D values of 41.6 ± 7.4 μM (ΔG = −5.98 ± 0.06 kcal/mol) for TES and 16.3 ± 0.5 μM (ΔG = − 6.53 ± 0.02 kcal/mol) for LCA, as estimated from a global analysis over 50 different wavelengths (Table S1). Both steroids bind OleP with an affinity comparable with the one determined for the physiological aglycone substrate DEO (23 ± 2 μM, ΔG = −6.32 ± 0.05 kcal/mol) in the same experimental conditions.[15] Nevertheless, binding to LCA elicits a 2-fold more pronounced spin shift of the heme iron to the high state in the spin equilibrium with respect to what is observed with TES and to what previously reported for DEO.[15] Indeed, the spectral transition induced by the binding of LCA at the maximum concentration explored (ΔAbs_{417nm}–0.07 au at 50 μM) is significantly higher than that observed with TES (ΔAbs_{417nm}–0.02 au at 200 μM) and DEO (ΔAbs_{417nm}–0.03 au at 80 μM,[15]), at saturating concentration. For a simple two-state equilibrium binding process, the larger is the amplitude of the transition the larger is the fraction of the P450 that is converted to the high spin state upon ligand binding.[21,22] The analysis of the high spin state content showed that, at equal concentration, TES binding determines only a minor population of OleP to shift toward the high spin state (~40%), while a largest high spin population is stabilized upon LCA binding (~60%) (Table S1). The difference in the amplitude of the observed spectral transition reflects the different ability of the substrate to displace the water molecule from the sixth coordinating position of the heme iron, favoring at the equilibrium the high spin pentacoordinate form. Therefore, the more pronounced spectral transition observed for LCA is attributable to a greater efficiency in displacing water and stabilizing the high spin form of the heme

Please cite this article in press as: Costanzo et al., Binding of steroid substrates reveals the key to the productive transition of the cytochrome P450 OleP, Structure (2024), https://doi.org/10.1016/j.str.2024.06.005

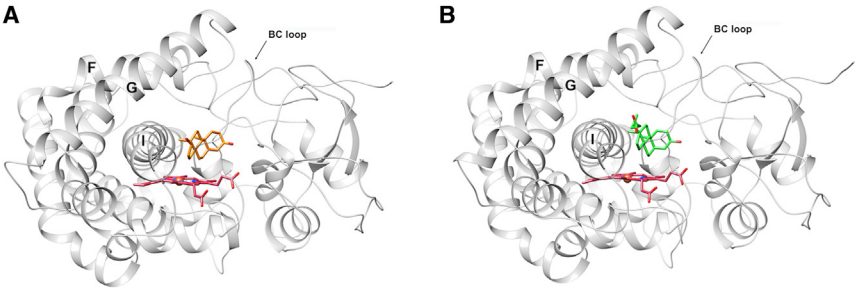

Figure 3. Steroid-bound OleP structures

OleP in complex with TES (A) or LCA (B), respectively shown in orange and green sticks. Both structures are displayed as light gray ribbons in a nonstandard orientation for P450s to allow a better visualization of the OleP active site closure. Helices F, G, and I and the loops BC and FG are labeled. See also Figure S2 and Table S2.

iron. This phenomenon in OleP is observed only when the substrate bound enzyme is in the closed conformation.[15–17,23] More precisely, previous structural data and binding kinetics experiments conducted with aglycone substrates indicate that substrate binding to OleP determines the formation of an heterogeneous ensemble of open and closed conformers.[15,16] Only in the closed state, the substrate can deeply penetrate the active site and displace the water molecule that coordinates the heme iron, stabilizing a high spin configuration. Therefore, it is reasonable to associate differences in type-I binding to the capability of the substrate to stabilize OleP in the closed state. Accordingly, these data indicate that the binding to LCA enhances the accumulation of the high spin pentacoordinate closed population of the LCA-OleP complex at the equilibrium. In contrast, the binding to TES only partially induces the shift to the closed high spin state, behaving similarly to the aglycone DEO, which we previously described as a sub-optimal substrate for OleP.[15]

Prompted by the observations highlighted previously, we conducted an additional equilibrium binding experiment in which we titrated steroid bound OleP solutions with increasing concentration of sodium formate. In fact, we previously demonstrated that an increase in the ionic strength shifts the open-closed equilibrium of the substrate bound OleP toward the closed state.[15–17,23] We worked at saturating concentration of the steroids. The result of this analysis shows that the increase in ionic strength enhances the spectroscopic signal of a high-spin heme iron either in the presence of LCA or TES, but the effect is steroid dependent (Figure S1). More precisely, while the effect of the ionic strength on the spin state equilibrium of LCA-OleP shows the total low-to-high spin shift at I ~ 2–2.5 M, in the presence of TES the shift is not complete even at the highest ionic strength conditions tested (I = 3.5 M). Considering that (i) the heme iron is high-spin pentacoordinate only in the closed state of the substrate-bound OleP[15,16] and that (ii) an increase in ionic strength shifts the conformational equilibrium of substrate bound OleP toward the closed state,[15–17,23] these results confirm the existence of a correlation between the enhanced spectroscopic signal of the high-spin species of LCA/TES-OleP and the increase of the closed population of LCA/TES-OleP. The different degree of the heme response to the ionic strength conditions may arise from a different capability of the steroid to affect the open-closed equilibrium. Therefore, the difference in the extent of the spectral shift induced by substrate binding and by the ionic strength variation indicates a different capability of the two steroids in stabilizing the closed conformation.

Overall structures

The structures of OleP bound to TES and to LCA were solved by X-ray crystallography at 2.3 Å resolution. Crystals were obtained by co-crystallization at high ionic strength conditions that are known to stabilize the enzyme in a closed conformation[15–17,23] and both structures were solved by molecular replacement. The refinement of the TES-OleP model gave R_{work} = 17.3% and R_{free} = 21.7%, whereas the refinement of LCA-OleP structure yielded R_{work} = 19.0% and R_{free} = 22.7% (Table S2). In both cases, the steroid-OleP complex is packed in a monoclinic space group containing six monomers per asymmetric unit. The six monomers superpose with a root-mean-square deviation (RMSD) of ~0.35 Å in TES-OleP and ~0.42 Å in LCA-OleP and show no major structural or conformational differences; therefore, unless otherwise indicated, we will discuss the structural features of monomer C of both complexes as it displays the lower average temperature factors (B-factors). All six monomers have been checked to ensure that all the structural features discussed are present, if allowed by the quality of the corresponding electron density map.

The initial electron density omit maps, calculated without inclusion of the steroid compounds in the models, revealed a clear electron density in the active site of the monomers populating the asymmetric unit corresponding to a single molecule of TES or LCA respectively in TES-OleP and LCA-OleP structures (Figure S2).

In complex with TES or LCA, OleP adopts a similar overall closed structure (overall RMSD on the Cα of about 0.20 Å) that resembles the one obtained with the physiological substrate DEO and the analog 6-deoxyerythronolide B (6DEB) under similar crystallization conditions (overall RMSD on the Cα of about 0.30 Å).[15,16] As previously described for the aglycone bound closed structures,[15,16] in both TES-OleP and LCA-OleP we observed that the internal helix I is bent and that the helix F, the helix G, and the loop connecting them are placed at the top of the active site, limiting the access of the external bulk (Figure 3).

TES and LCA in the OleP active site

The analysis of the active site of both complexes allowed the identification of typical features of the catalytically competent closed structure of OleP [6,7]. Indeed, the position adopted by both TES and LCA within the distal site induces the displacement of the sixth iron coordinating water molecule yielding a pentacoordinate heme in both complexes.

In addition, the establishment of van der Waals contacts with the helix I determines the rupture of the helical geometry at the

Please cite this article in press as: Costanzo et al., Binding of steroid substrates reveals the key to the productive transition of the cytochrome P450 OleP, Structure (2024), https://doi.org/10.1016/j.str.2024.06.005

CellPress
OPEN ACCESS

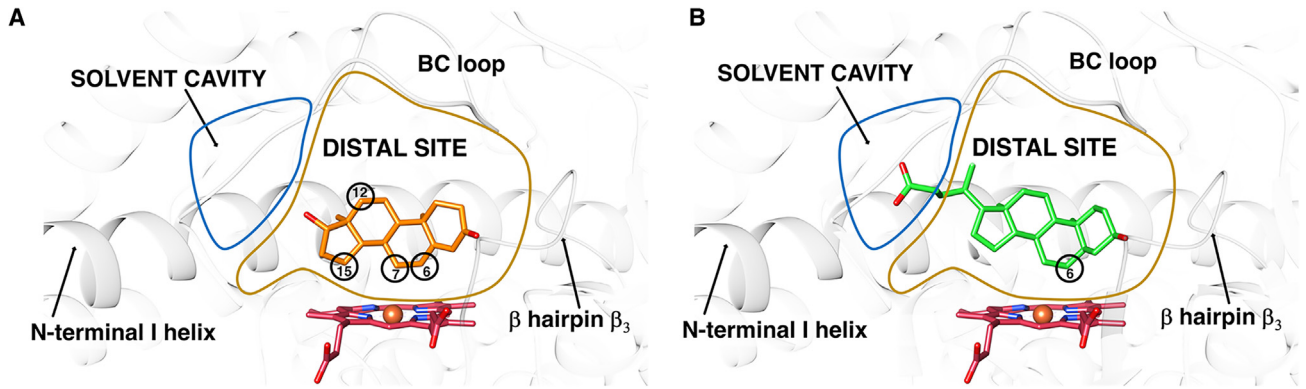

Figure 4. TES and LCA in the active site of OleP

Close-up view of the active site found in TES-OleP (A) and LCA-OleP (B) structures. Gold and light blue lines schematically outline the distal site and the solvent cavity. TES, LCA, and the heme are shown as orange, green, and red sticks, respectively. The targets of the OleP reaction on the two substrates are labeled and circled. See also Figure S3.

level of the central 244–248 turn of the helix I, with the consequent formation of a small catalytic cleft. This structural element is commonly considered a crucial support for the proton transfer process toward the active site occurring during the catalytic reaction (Figure S3).[24]

In the closed state, two major cavities can be distinguished within the active site of OleP: the main cavity that corresponds to the distal site with respect to the heme, and the solvent cavity, a small chamber that is enclosed by the helix I, the BC loop, and the bound substrate (Figure 4).[15–17]

The superposition of the six monomers found in the asymmetric unit showed that in the high ionic strength conditions resulting in the crystallization of the enzyme in the closed state, both substrates arrange in a unique and similar pose within the OleP active site. TES and LCA are both placed parallel to the helix I, with the B, C, and D rings facing the helix; the steroidal core is disposed perpendicular to the tetra porphyrin ring with the β-face oriented toward the heme iron. This position enables the pentanoic acid chain of LCA to extend over the solvent cavity (Figure 4). In LCA-OleP complex we found the C6 of the substrate directed toward the heme iron and placed at about 4.5 Å, whereas the other LCA carbons are located at least 5 Å away from the iron. This represents an optimal position for the regioselective catalysis and it is consistent with the observation of a mono-site hydroxylation of LCA.[19] In agreement with the C6 and C7 hydroxylated products described by Agematu et al.,[18] in TES-OleP, we observed that carbons 6 and 7 of TES are directed toward the heme iron and placed at a distance compatible with the catalytic event (~4.7 Å), the other carbons being located at distances above 5.7 Å (Figure 4).

Within the active site of OleP both substrates establish a network of van der Waals interactions with the side chains of residues exposed to the distal site and belonging to the loop BC (E89, G92, and L94), the helix F (M178 and L179), the helix I (I243, A244, and T248), the β-hairpin β3 (V291), and the β-hairpin β4 (L396 and I397) (Figure 5). Moreover, both molecules form a carbonyl-aromatic interaction with the ketone group at the C3 and F321 (helix K′).

In addition to those contacts, the molecule of TES establishes a direct hydrogen-bond with S240 at the N-terminus of helix I through its hydroxyl group at the C17, facing the solvent cavity. For its part, the molecules of LCA with its acidic function are involved in a strong dipole-dipole interaction with the side chain of N236 and in a hydrogen bond with S240 at the N-terminus of helix I. The chain of pentanoic acid with the carboxylic group is also hydrogen bonded with the backbone of E89 and G92 (BC loop), resulting fully inserted into the solvent cavity (Figure 5).

Along with the direct interactions, we identified enzyme-substrate indirect contacts, mediated by solvent molecules, that are similar for the two structures since they involve the steroidal nucleus. These interactions enable the steroid substrates to interact with the β-hairpin β3, the β-hairpin β4, and the loop BC. In particular in TES-OleP we found that water molecules mediate (i) the interaction between the A-ring of TES and F84 (BC loop) and F296 (β-hairpin β3); (ii) the contact between the ketone group at C3 and A293, G294, S295, and the amino group of the F296 (β-hairpin β3) together with the contact with one of the heme propionates; and (iii) the interaction between the hydroxyl group at C17 and E89, V93, L94, and A95 (BC loop) (Figure 6).

Similarly in LCA-OleP we found that (i) one formate ion, coming from the crystallization buffer, and one water molecule mediate the interaction between the A-, C-, and D-rings of LCA with F84 (BC loop) and F296 (β -hairpin β3); (ii) the hydroxyl group at the C3 interacts with the carbonyl of the main chain of A293, G294, S295, and the amino group of the F296 (β-hairpin β3), with F84 (BC loop), together with one of the heme propionates through water molecules; (iii) the pentanoic acid at the C17 interacts with the backbone of E89 (BC loop) and F296 (β-hairpin β3) through water and a formate ion (Figure 6). Of note, the same pattern of contacts was described in the structure of DEO-OleP complex, but, in this case, there are no bridging solvent molecules, as the substrate is directly involved in those interactions.[15]

Direct contacts with the N-terminal residues of helix I provide an efficient trigger for the OleP closure and contribute to the selectivity of the reaction

In an effort to provide a structural explanation for the spectral behavior observed in the binding experiments and to determine the reasons for the different reactivity reported against the two

Please cite this article in press as: Costanzo et al., Binding of steroid substrates reveals the key to the productive transition of the cytochrome P450 OleP, Structure (2024), https://doi.org/10.1016/j.str.2024.06.005

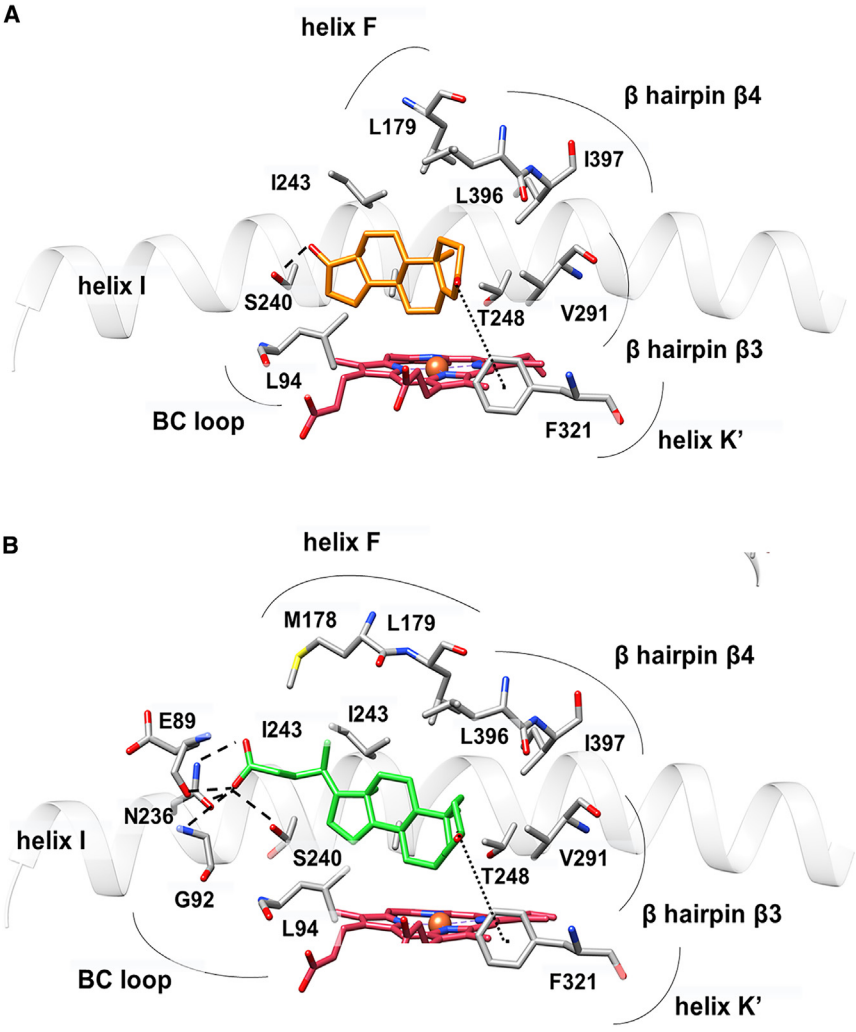

Figure 5. Direct contacts between OleP and steroids

The active sites found in TES-OleP (A) and LCA-OleP (B) structure are reported, and the secondary structural elements are indicated. Residues involved in direct contacts within 5 Å of distance with the steroidal substrates are shown as dark gray sticks and labeled. Multiple conformers are shown, the transparency indicate the less represented conformers found in the asymmetric unit among the six monomers. The helix I is shown as a light gray ribbon. Dashed lines indicate hydrogen bonds. TES, LCA, and heme are in orange, green, and red sticks, respectively.

steroidal compounds, the active site structure of TES-OleP was compared with that of LCA-OleP. As described previously, the major discriminating element between TES and LCA is the substituent group at the C17, which in the case of LCA is a chain of pentanoic acid (Figure 1). The superposition of the two steroid-bound OleP structures shows that the presence of this substituent induces a displacement of the side chain of E89 on the BC loop, which rotates about 90° with respect to the position observed in TES-OleP. This rearrangement enables the accommodation of the pentanoic acid chain of LCA inside the solvent cavity, which forms direct hydrogen bonds with the side chains of S240 and N236 at the N-terminus of the helix I. Conversely, the TES molecule cannot reach the solvent cavity: the presence of a short hydroxyl group at C17 only enables the formation of a single direct contact with S240, external to the cavity (Figure 7).

This structural difference may explain the different binding properties observed with TES and LCA in solution in physiological ionic strength conditions (I∼ 0.2 M) and upon ionic strength variations. Indeed, we previously postulated that the establishment of direct hydrogen bonds between the substrate and N236 and S240 at the N-terminus of the helix I are at the basis of the activation of the molecular mechanism that leads the enzyme to close, adopting the catalytically competent state with a pentacoordinate high-spin heme iron.[15] Therefore, the capability of LCA to directly interact with those residues enables the activation of the mechanism of closure of OleP more efficiently, favoring the transition to the high spin state that results in a more pronounced type I spectral change. On the contrary, the presence of a single direct interaction with S240, as observed with TES, only occasionally induces the conformational transition and the spin state shift. We may surmise that under physiological conditions, the conformational distribution of the TES-OleP complex favors the unproductive open state at equilibrium. Therefore, the lower magnitude of the spectral changes observed in the equilibrium binding assays may be due to a looser binding of TES that results in a minor effect of this substrate on the overall transition toward the closed high spin state.

The very same interactions, in conjunction with the contacts established within the distal site, could favor the stabilization of a unique position of the substrate in the OleP active site, providing a strong contribution to the high regioselectivity observed with LCA.[19] In LCA-OleP, the C6 is perfectly β-oriented toward the metal center and placed at an optimal distance for the catalytic reaction. The stabilization of this position, which is accompanied by the closure of the active site, allows the enzyme to carry out the C6β-hydroxylation with high regioselectivity. On the contrary, the absence of these interactions can be associated with the scarce selectivity observed in the reaction with TES.[18] Indeed, together with the C6 hydroxylated products, other hydroxylated derivatives at C7, C12, and C15 were identified. Our structural analysis shows that the pose adopted by TES when the enzyme is in the closed conformation enables both the C6 and C7 centers to occupy a suitable position and orientation for catalysis, potentially favoring the reaction on these two targets to the same extent. In the latter condition, the reactions on the C12 and C15 are unfavorable, being the C12 on the opposite side of the molecule with respect to the heme iron and the

Please cite this article in press as: Costanzo et al., Binding of steroid substrates reveals the key to the productive transition of the cytochrome P450 OleP, Structure (2024), https://doi.org/10.1016/j.str.2024.06.005

CellPress
OPEN ACCESS

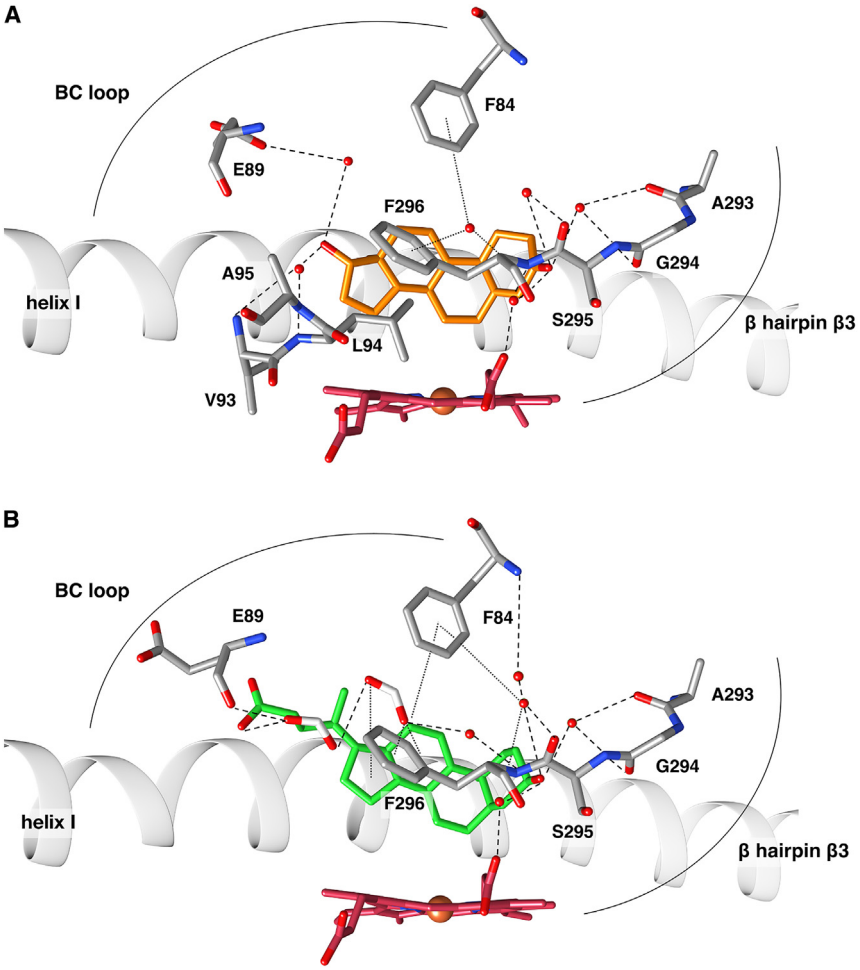

Figure 6. Indirect contacts between OleP and steroids

Close up view of the active site of TES-OleP (A) and LCA-OleP (B) structures. Residues involved in indirect contacts with the steroidal substrates are labeled and shown as dark gray sticks. Secondary structural elements are also indicated. The helix I is shown as a light gray ribbon. Dashed lines indicate hydrogen bonds. Thin dashed lines indicate dipole-dipole interactions. Red spheres are water molecules, white sticks represent formate ions. TES, LCA, and heme are in orange, green, and red sticks, respectively.

C15 too far from the active center (>6 Å) (Figure 4). These observations are in agreement with the functional analysis performed by Agematu et al.,[18] which reports a conversion rate above 10% for the 6β- and the 7β-hydroxylated derivatives, and between 5 and 10% for the 12β- and the 15β-hydroxylated products. We may assume that in solution, under physiological-like ionic strength conditions (I∼ 0.2 M), in the TES-bound closed OleP, the absence of contacts with the solvent cavity, not even mediated by solvent molecules, may release TES from the constraints enforced by the closed conformation. This may enable the substrate to adopt alternative poses with respect to the one observed in the crystal that promotes hydroxylation reactions on alternative centers, such as C12 and C15.

To further explore the stability of the poses of the steroidal substrates found in the crystal structures, we carried out MD simulations on both complexes. The analysis of the atomic distances between the iron (Fe) atom and the C6/C7 of LCA and TES showed a higher stability of the pose of LCA, with the most probable distance sampled centered at 4.4 Å and 5.5 Å for Fe-C6 and Fe-C7, respectively (Figure 8). The same distances in the TES-OleP complex are both shifted to larger values, i.e., 5.1 Å and 6.5 Å, and, thus, reactive-like conformations are less sampled. In addition, the distributions of these distances are broader in the case of TES, confirming the different behavior compared to LCA. The analysis of the average distance between each atom of the ligand, excluding hydrogens, and the neighboring residues allowed us to identify the most stable interactions in both complexes. In the case of LCA, we identified 47 interactions that maintained an average value less or equal to 5 Å while in TES-OleP complex more than 10 interactions are lost (Figure S4). The number of protein-ligand hydrogen bonds, which is higher in the presence of LCA, follows a similar trend, which reflects the stability of the non-covalent binding pose (Figure S5). Overall, the results of the simulations confirm that TES exhibits greater flexibility within the active site of OleP compared to LCA, providing additional evidence to delineate the molecular basis of the high selectivity of the enzyme toward the latter substrate.

It is of interest to comment on the way solvent molecules rearrange inside the active site of the enzyme in response to the different bound substrates. To better analyze this aspect, we compared the steroid-bound structures with the one of OleP bound to DEO obtained in analogous crystallization conditions[15] (Figure 9).

The presence of the lactonic macrocycle of the aglycone DEO substrate in the distal site determines the displacement of solvent molecules and their accumulation into the solvent cavity (Figure 9·[15]). Of note, solvent molecules occupy the exact same positions in other macrolide-bound structures of OleP (PDB: 5MNS,[16] PDB: 6ZHZ, 6ZI7, and 6ZI3[15]), occurring in over 90% of cases. On the other hand, the binding of LCA or TES promotes the displacement of solvent molecules from the solvent cavity and their accumulation to the portion of the distal site that the structure of steroid substrates cannot occupy, namely the one facing the loop BC, the β-hairpin β3, and the β-hairpin β4. The positions adopted by these molecules are not random; they repeat themselves in a nearly identical manner within the six copies of the crystallographic asymmetric unit. The B-factors of these molecules are comparable to the average B-factors calculated for the whole protein, the heme, and the bound ligand, with the sole exception of the formate ions found in the LCA structure, whose values exceed of a 30% (Table S3). In addition, we found that four waters connecting the carbonyl group in C3 with the segment 293–296 (β-hairpin β3) occupy the same positions in

Please cite this article in press as: Costanzo et al., Binding of steroid substrates reveals the key to the productive transition of the cytochrome P450 OleP, Structure (2024), https://doi.org/10.1016/j.str.2024.06.005

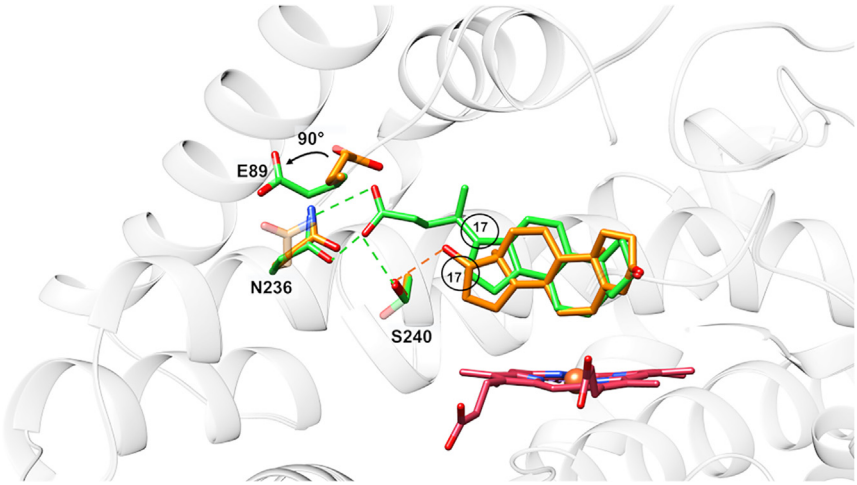

Figure 7. Differences in TES and LCA binding modes

Superposition of the active sites of TES-OleP and LCA-OleP (light gray ribbon). E89 (BC loop), N236, and S240 (helix I) are labeled and shown as orange (TES-OleP) and green (LCA-OleP) sticks. Multiple conformers of N236 and S240 are shown, the transparency indicate the less represented conformers found in the asymmetric unit among the six monomers. TES, LCA, and the heme are in orange, green, and red sticks, respectively. Orange and green dashed lines indicate the respective hydrogen bonds identified in TES-OleP and LCA-OleP.

both structures (Figures 6 and 9). These observations lead us to conclude that the solvent molecules trapped in the closed active site of OleP play a structural role. They move in the active site following the shape of the bound substrate and accumulate, structuring, in zones that the substrate cannot fill, mediating and optimizing the interactions with the enzyme. The role of structured solvent molecules within the active site of ligand-bound P450s has been previously described by Conner et al.[25] as a mechanism utilized by multifunctional P450s that may serve to enhance their substrate versatility. We believe that OleP represents an excellent example in this sense. Differently to other P450s where order among internal water molecules seems to be primarily influenced by hydrophobic solvation upon the entrance of hydrophobic substrates in the active site,[26,27] in the case of OleP the nature of the substrate contributes to the structuring of solvent molecules. This observation suggests the existence of an intricate interplay between substrate properties and solvent organization in the OleP active site and supports previous hypotheses that attribute its broad substrate specificity to ordered solvent molecules[15]; these molecules rearrange in the active site compensating for the absence of structural elements of the substrate, also favoring the establishment of productive interactions with non-specific ligands.

Additionally, these findings show that the presence of solvent mediated interactions enables the accommodation of different substrates such as DEO, TES, and LCA, that are differently positioned inside the distal pocket of OleP and establish different types of interactions with the enzyme, to form the same overall pattern of substrate-P450 contacts, involving the same portions of the protein and the same exposed amino acidic residues of the active site. This might explain the reason for the small differences found in the binding affinity of OleP with these substrates.

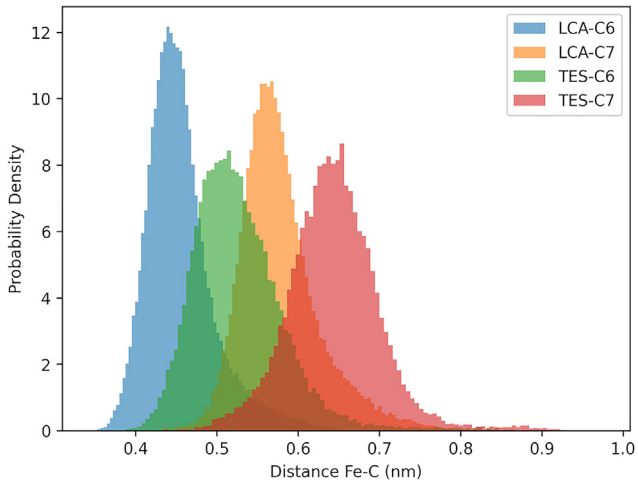

Figure 8. Stability of the pose of LCA and TES bound to OleP

The distribution of the distances between the Fe atom and the C6/C7 of LCA and TES, along the MD simulations, are represented. See also Figure S4 and Figure S5.

Conclusions

The structural analysis of OleP bound to TES and LCA reported in this work, integrated with binding affinity assays and MD simulations, provides clues to clarify the molecular mechanism at the basis of the regulation of the open-to-closed structural transition induced by substrate binding that leads the enzyme to achieve the productive conformation.

The comparison of the crystal structures of OleP bound to TES and LCA, interpreted in the light of the results of the binding assays, confirmed the importance of the establishment of direct hydrogen bonds between the substrate and both N236 and S240 residues at the N-terminus of the helix I of OleP in efficiently activating the structural transition. The direct contact with these amino acids more frequently promotes the approach of the N-terminal portion of the helix I to the substrate, favoring its bending. This movement pulls the entire FG unit over the active site, stabilizing the closed structure and favoring the high-spin accumulation at the equilibrium of the LCA-OleP species, as indicated by binding assays. The sole interaction with S240 which is provided by the hydroxyl function at the C17 of TES is not sufficient to exert a firm trigger for the active site closure. This results in a minor accumulation of TES-OleP high-spin closed population at the equilibrium, as indicated by a lower magnitude of the spectral transition observed in the binding experiments. Similar to what was observed comparing the OleP physiological substrates DEO and L-O-DEO,[15] these results show that the presence of a substrate endowed with structural elements that enable the simultaneous direct contact with the distal site and the solvent

Please cite this article in press as: Costanzo et al., Binding of steroid substrates reveals the key to the productive transition of the cytochrome P450 OleP, Structure (2024), https://doi.org/10.1016/j.str.2024.06.005

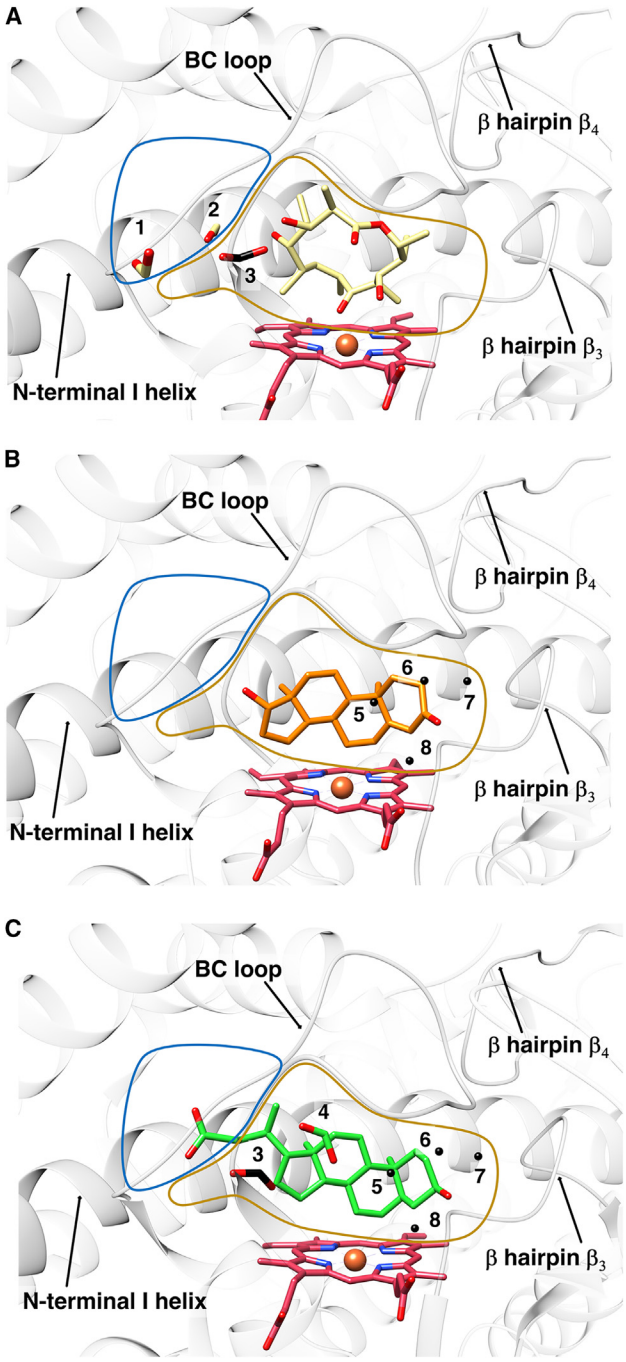

Figure 9. Rearrangement of solvent molecules within the active site of OleP in response to different bound substrates

Close up view of the active site of DEO-OleP (PDB ID 6ZHZ[15]) (A), TES-OleP (B), LCA-OleP (C). Gold and light blue lines schematically outline the distal site and the solvent cavity. The OleP structure is shown as light gray ribbon. DEO, TES, LCA, and heme are represented as khaki, orange, green, and red sticks. Waters and formate ions that mediate the substrate-OleP interactions are shown as spheres and sticks, respectively. Solvent molecules that are in the same positions in all the three structures are colored in black, those found in a single structure are colored according to the color of the relative ligand. The positions where solvent molecules were found in the structures are numbered. Positions 1–3 locate within the solvent cavity (blue lines) while positions 4–8 are in the distal site (gold lines). See also Table S3.

cavity determines the activation of the molecular mechanism that induces the closure of the active site.

In the broader context of steroid converting P450s, this work enabled the identification of the structural determinants for the gain in regio- and stereoselectivity of a native P450.[28] The comparative structural analysis here discussed revealed that the substituent group at C17 influences the selectivity of the hydroxylation reaction catalyzed by OleP.

Among the bacterial P450s that are natively able to introduce hydroxyl functions to steroidal compounds,[28] few are those structurally characterized in a productive steroid-bound form. In these structures, the bound steroid molecules vertically traverse the active site in a perpendicular orientation compared to the heme, exposing a single stereogenic center to the heme iron at a distance compatible with catalysis. This is exemplified by the steroid-bound structures of members of the CYP154 and CYP109 families.[29–33] The closed structure adopted by these enzymes upon steroid binding presents a hydrophobic channel where the steroid binds that restricts the molecule from assuming multiple conformations, thereby elucidating the basis for the high regio- and stereoselectivity of the hydroxylation reaction observed. Due to differences in shape and volume of the active site and of the nature and the distribution of the substrate binding residues, we found an alternative arrangement of steroidal compounds in OleP. In the latter case, the steroid horizontally traverses the active site and exposes multiple stereogenic centers to the heme iron at the same time. The disadvantage of this pose is that it does not guarantee selectivity unless the steroid can simultaneously contact the two cavities of the OleP active site. Nevertheless, an appropriate selection of the steroidal molecule, such as esterified derivatives of TES, and/or a rational approach of protein engineering could potentially yield an enzyme capable of catalyzing stereo- and regioselective reactions on different stereogenic centers. To conclude, the results presented in this work clarify key aspects of the regulation of the substrate binding mechanism of OleP and provide a description of critical elements that contribute to the selectivity of the catalytic reaction. In the context of the emerging interest in the use of cytochrome P450s as biocatalysts for the regio- and stereoselective hydroxylation of steroidal compounds,[5,34,35] the structural description of OleP bound to TES and LCA paves the way for future works aimed at designing engineered variants of the P450 endowed with enhanced regio- and stereoselectivity of hydroxylation toward highly valuable steroids. In this perspective, rational engineering of OleP based on the information obtained in this work could enable the optimization of the regioselective 7β-hydroxylation of LCA performed by a newly developed engineered form of OleP,[36] and/or the development of regioselective forms of the enzyme for the 6β- or 7β-hydroxylated derivatives of TES, representing an alternative strategy to produce compounds with interesting therapeutic applications as neuroprotective and anti-inflammatory agents.

STAR★METHODS

Detailed methods are provided in the online version of this paper and include the following:

- KEY RESOURCES TABLE
- RESOURCE AVAILABILITY
  - Lead contact

SUPPLEMENTAL INFORMATION

Supplemental information can be found online at https://doi.org/10.1016/j.str.2024.06.005.

ACKNOWLEDGMENTS

This project has received funding from the European Union's Horizon 2020 research and innovation program under the Marie Skłodowska-Curie grant agreement no. 823780 and the Italian MUR-PRIN 2022, 2022HREZJT_LS1 to B.V.; the Italian MUR-PRIN 2020, 2020PKLEPN_LS3, and 2022, 202288TXLY_PE3 to L.C.M. This work was supported by the research project "Potentiating the Italian Capacity for Structural Biology Services in Instruct Eric" (Acronym: ITACA.SB, project no. IR0000009) within the call MUR D.D. 0003264 dated 28/12/2021 PNRR M4/C2/L3.1.1, funded by the European Union NextGenerationEU. We acknowledge Elettra Sincrotrone Trieste for providing access to its synchrotron radiation facilities and we thank Nicola Demitri and Annie Heroux for assistance in using beamline XRD2.

AUTHOR CONTRIBUTIONS

Conceptualization, B.V., C.S., and L.C.M.; methodology, A.C., F.F., I.F., M.D.S., M.D., B.V., C.S., and L.C.M.; validation, B.V., C.S., and L.C.M.; formal analysis, A.C., F.F., and L.C.M.; investigation, A.C., F.F., I.F., M.D.S., E.G., G.B., M.D.R., L.B., C.E., G.P., and M.D.; resources, B.V. and L.C.M.; data curation, A.C., F.F., I.F., M.D.S., M.D., B.V., C.S., and L.C.M.; writing—original draft preparation, A.C., F.F., and L.C.M.; writing—review and editing, A.C., F.F., I.F., C.E., B.V., C.S., and L.C.M.; visualization, A.C., F.F., M.D.S., and L.C.M.; supervision, B.V., C.S., and L.C.M.; project administration, B.V., C.S., and L.C.M.; funding acquisition, B.V. and L.C.M. All authors have read and agreed to the published version of the manuscript.

DECLARATION OF INTERESTS

The authors declare no competing interests.

Received: January 5, 2024
Revised: May 8, 2024
Accepted: June 11, 2024
Published: July 5, 2024

REFERENCES

1. Donova, M. (2021). Microbial Steroid Production Technologies: Current Trends and Prospects. Microorganisms *10*, 53. https://doi.org/10.3390/microorganisms10010053.
2. Ericson-Neilsen, W., and Kaye, A.D. (2014). Steroids: pharmacology, complications, and practice delivery issues. Ochsner J. *14*, 203–207.
3. Ke, S. (2018). Recent Progress of Novel Steroid Derivatives and Their Potential Biological Properties. Mini Rev. Med. Chem. *18*, 745–775. https://doi.org/10.2174/1389557517666171003103245.
4. Li, Z., Van Beilen, J.B., Duetz, W.A., Schmid, A., De Raadt, A., Griengl, H., and Witholt, B. (2002). Oxidative biotransformations using oxygenases. Curr. Opin. Chem. Biol. *6*, 136–144. https://doi.org/10.1016/S1367-5931(02)00296-X.
5. Zhang, X., Hu, Y., Peng, W., Gao, C., Xing, Q., Wang, B., and Li, A. (2021). Exploring the Potential of Cytochrome P450 CYP109B1 Catalyzed Regio- and Stereoselective Steroid Hydroxylation. Front. Chem. *9*, 649000. https://doi.org/10.3389/fchem.2021.649000.
6. Bureik, M., and Bernhardt, R. (2007). Steroid Hydroxylation: Microbial Steroid Biotransformations Using Cytochrome P450 Enzymes. In Modern Biooxidation, R.D. Schmid and V.B. Urlacher, eds. (Wiley), pp. 155–176. https://doi.org/10.1002/9783527611522.ch6.
7. Donova, M.V. (2017). Steroid Bioconversions. In Microbial Steroids Methods in Molecular Biology, J.-L. Barredo and I. Herráiz, eds. (New York: Springer), pp. 1–13. https://doi.org/10.1007/978-1-4939-7183-1_1.
8. Li, Z., Jiang, Y., Guengerich, F.P., Ma, L., Li, S., and Zhang, W. (2020). Engineering cytochrome P450 enzyme systems for biomedical and biotechnological applications. J. Biol. Chem. *295*, 833–849. https://doi.org/10.1074/jbc.REV119.008758.
9. Durairaj, P., Hur, J.-S., and Yun, H. (2016). Versatile biocatalysis of fungal cytochrome P450 monooxygenases. Microb. Cell Fact. *15*, 125. https://doi.org/10.1186/s12934-016-0523-6.
10. Shah, S., Xue, Q., Tang, L., Carney, J.R., Betlach, M., and McDaniel, R. (2000). Cloning, characterization and heterologous expression of a polyketide synthase and P-450 oxidase involved in the biosynthesis of the antibiotic oleandomycin. J. Antibiot. (Tokyo) *53*, 502–508. https://doi.org/10.7164/antibiotics.53.502.
11. Tatsuta, K., Gunji, H., Tajima, S., Ishiyama, T., Imai, S., Okuyama, S., and Fukatsu, S. (1990). Biosynthetic studies on oleandomycin by incorporation of the chemically synthesized aglycones. J. Antibiot. (Tokyo) *43*, 909–911. https://doi.org/10.7164/antibiotics.43.909.
12. Rodriguez, A.M., Olano, C., Méndez, C., Hutchinson, C.R., and Salas, J.A. (1995). A cytochrome P450-like gene possibly involved in oleandomycin biosynthesis by Streptomyces antibioticus. FEMS Microbiol. Lett. *127*, 117–120. https://doi.org/10.1111/j.1574-6968.1995.tb07459.x.
13. Gaisser, S., Lill, R., Staunton, J., Méndez, C., Salas, J., and Leadlay, P.F. (2002). Parallel pathways for oxidation of 14-membered polyketide macrolactones in Saccharopolyspora erythraea. Mol. Microbiol. *44*, 771–781. https://doi.org/10.1046/j.1365-2958.2002.02910.x.
14. Schröder, G.C., Smit, M.S., and Opperman, D.J. (2023). Harnessing heme chemistry: Recent advances in the biocatalytic applications of cytochrome P450 monooxgenases. Curr. Opin. Green Sustain. Chem. *39*, 100734. https://doi.org/10.1016/j.cogsc.2022.100734.
15. Parisi, G., Freda, I., Exertier, C., Cecchetti, C., Gugole, E., Cerutti, G., D'Auria, L., Macone, A., Vallone, B., Savino, C., and Montemiglio, L.C. (2020). Dissecting the Cytochrome P450 OleP Substrate Specificity: Evidence for a Preferential Substrate. Biomolecules *10*, 1411. https://doi.org/10.3390/biom10101411.
16. Parisi, G., Montemiglio, L.C., Giuffrè, A., Macone, A., Scaglione, A., Cerutti, G., Exertier, C., Savino, C., and Vallone, B. (2019). Substrate-induced conformational change in cytochrome P450 OleP. FASEB J. *33*, 1787–1800. https://doi.org/10.1096/fj.201800450RR.
17. Montemiglio, L.C., Gugole, E., Freda, I., Exertier, C., D'Auria, L., Chen, C.G., Nardi, A.N., Cerutti, G., Parisi, G., D'Abramo, M., et al. (2021). Point Mutations at a Key Site Alter the Cytochrome P450 OleP Structural Dynamics. Biomolecules *12*, 55. https://doi.org/10.3390/biom12010055.
18. Agematu, H., Matsumoto, N., Fujii, Y., Kabumoto, H., Doi, S., Machida, K., Ishikawa, J., and Arisawa, A. (2006). Hydroxylation of testosterone by bacterial cytochromes P450 using the Escherichia coli expression system. Biosci. Biotechnol. Biochem. *70*, 307–311. https://doi.org/10.1271/bbb.70.307.
19. Grobe, S., Wszołek, A., Brundiek, H., Fekete, M., and Bornscheuer, U.T. (2020). Highly selective bile acid hydroxylation by the multifunctional bacterial P450 monooxygenase CYP107D1 (OleP). Biotechnol. Lett. *42*, 819–824. https://doi.org/10.1007/s10529-020-02813-4.

20. Isin, E.M., and Guengerich, F.P. (2008). Substrate binding to cytochromes P450. Anal. Bioanal. Chem. *392*, 1019–1030. https://doi.org/10.1007/s00216-008-2244-0.

21. Mak, P.J., and Denisov, I.G. (2018). Spectroscopic studies of the cytochrome P450 reaction mechanisms. Biochim. Biophys. Acta. Proteins Proteom. *1866*, 178–204. https://doi.org/10.1016/j.bbapap.2017.06.021.

22. Jung, C., Ristau, O., and Rein, H. (1991). The high-spin/low-spin equilibrium in cytochrome P-450–a new method for determination of the high-spin content. Biochim. Biophys. Acta *1076*, 130–136. https://doi.org/10.1016/0167-4838(91)90229-s.

23. De Sciscio, M.L., Nardi, A.N., Parisi, G., Bulfaro, G., Costanzo, A., Gugole, E., Exertier, C., Freda, I., Savino, C., Vallone, B., et al. (2023). Effect of Salts on the Conformational Dynamics of the Cytochrome P450 OleP. Molecules *28*, 832. https://doi.org/10.3390/molecules28020832.

24. Cupp-Vickery, J.R., Garcia, C., Hofacre, A., and McGee-Estrada, K. (2001). Ketoconazole-induced conformational changes in the active site of cytochrome P450eryF. J. Mol. Biol. *311*, 101–110. https://doi.org/10.1006/jmbi.2001.4803.

25. Conner, K.P., Woods, C.M., and Atkins, W.M. (2011). Interactions of cytochrome P450s with their ligands. Arch. Biochem. Biophys. *507*, 56–65. https://doi.org/10.1016/j.abb.2010.10.006.

26. Johnston, J.B., Kells, P.M., Podust, L.M., and Ortiz De Montellano, P.R. (2009). Biochemical and structural characterization of CYP124: A methyl-branched lipid ω-hydroxylase from *Mycobacterium tuberculosis*. Proc. Natl. Acad. Sci. USA *106*, 20687–20692. https://doi.org/10.1073/pnas.0907398106.

27. Cryle, M.J., and Schlichting, I. (2008). Structural insights from a P450 Carrier Protein complex reveal how specificity is achieved in the P450 $_{Biol}$ ACP complex. Proc. Natl. Acad. Sci. USA *105*, 15696–15701. https://doi.org/10.1073/pnas.0805983105.

28. Zhang, J., Liu, Y., Zheng, Y., Luo, Y., Du, Y., Zhao, Y., Guan, J., Zhang, X., and Fu, J. (2020). TREM-2-p38 MAPK signaling regulates neuroinflammation during chronic cerebral hypoperfusion combined with diabetes mellitus. J. Neuroinflammation *17*, 2. https://doi.org/10.1186/s40643-019-0290-4.

29. Herzog, K., Bracco, P., Onoda, A., Hayashi, T., Hoffmann, K., and Schallmey, A. (2014). Enzyme-substrate complex structures of CYP154C5 shed light on its mode of highly selective steroid hydroxylation. Acta Crystallogr. D Biol. Crystallogr. *70*, 2875–2889. https://doi.org/10.1107/S1399004714019129.

30. Bracco, P., Wijma, H.J., Nicolai, B., Buitrago, J.A.R., Klünemann, T., Vila, A., Schrepfer, P., Blankenfeldt, W., Janssen, D.B., and Schallmey, A. (2021). CYP154C5 Regioselectivity in Steroid Hydroxylation Explored by Substrate Modifications and Protein Engineering. Chembiochem *22*, 1099–1110. https://doi.org/10.1002/cbic.202000735.

31. Dangi, B., Lee, C.W., Kim, K.-H., Park, S.-H., Yu, E.-J., Jeong, C.-S., Park, H., Lee, J.H., and Oh, T.-J. (2019). Characterization of two steroid hydroxylases from different Streptomyces spp. and their ligand-bound and -unbound crystal structures. FEBS J. *286*, 1683–1699. https://doi.org/10.1111/febs.14729.

32. Gao, Q., Ma, B., Wang, Q., Zhang, H., Fushinobu, S., Yang, J., Lin, S., Sun, K., Han, B.-N., and Xu, L.-H. (2023). Improved 2α-Hydroxylation Efficiency of Steroids by CYP154C2 Using Structure-Guided Rational Design. Appl. Environ. Microbiol. *89*, e0218622. https://doi.org/10.1128/aem.02186-22.

33. Zhang, X., Shen, P., Zhao, J., Chen, Y., Li, X., Huang, J.-W., Zhang, L., Li, Q., Gao, C., Xing, Q., et al. (2023). Rationally Controlling Selective Steroid Hydroxylation via Scaffold Sampling of a P450 Family. ACS Catal. *13*, 1280–1289. https://doi.org/10.1021/acscatal.2c04906.

34. Ma, B., Wang, Q., Ikeda, H., Zhang, C., and Xu, L.-H. (2019). Hydroxylation of Steroids by a Microbial Substrate-Promiscuous P450 Cytochrome (CYP105D7): Key Arginine Residues for Rational Design. Appl. Environ. Microbiol. *85*, e01530-19. https://doi.org/10.1128/AEM.01530-19.

35. Pardhe, B.D., Kwon, K.P., Park, J.K., Lee, J.H., and Oh, T.-J. (2023). H2O2-Driven Hydroxylation of Steroids Catalyzed by Cytochrome P450 CYP105D18: Exploration of the Substrate Access Channel. Appl. Environ. Microbiol. *89*, e0158522. https://doi.org/10.1128/aem.01585-22.

36. Grobe, S., Badenhorst, C.P.S., Bayer, T., Hamnevik, E., Wu, S., Grathwol, C.W., Link, A., Koban, S., Brundiek, H., Großjohann, B., and Bornscheuer, U.T. (2021). Engineering Regioselectivity of a P450 Monooxygenase Enables the Synthesis of Ursodeoxycholic Acid via 7β-Hydroxylation of Lithocholic Acid. Angew. Chem. Int. Ed. *60*, 753–757. https://doi.org/10.1002/anie.202012675.

37. Montemiglio, L.C., Parisi, G., Scaglione, A., Sciara, G., Savino, C., and Vallone, B. (2016). Functional analysis and crystallographic structure of clotrimazole bound OleP, a cytochrome P450 epoxidase from Streptomyces antibioticus involved in oleandomycin biosynthesis. Biochim. Biophys. Acta *1860*, 465–475. https://doi.org/10.1016/j.bbagen.2015.10.009.

38. Kabsch, W. (2010). XDS. Acta Crystallogr. D Biol. Crystallogr. *66*, 125–132. https://doi.org/10.1107/S0907444909047337.

39. Collaborative Computational Project Number 4 (1994). The CCP4 suite: programs for protein crystallography. Acta Crystallogr. D Biol. Crystallogr. *50*, 760–763. https://doi.org/10.1107/S0907444994003112.

40. Emsley, P., and Cowtan, K. (2004). *Coot* : model-building tools for molecular graphics. Acta Crystallogr. D Biol. Crystallogr. *60*, 2126–2132. https://doi.org/10.1107/S0907444904019158.

41. Chen, V.B., Arendall, W.B., Headd, J.J., Keedy, D.A., Immormino, R.M., Kapral, G.J., Murray, L.W., Richardson, J.S., and Richardson, D.C. (2010). *MolProbity* : all-atom structure validation for macromolecular crystallography. Acta Crystallogr. D Biol. Crystallogr. *66*, 12–21. https://doi.org/10.1107/S0907444909042073.

42. Williams, C.J., Headd, J.J., Moriarty, N.W., Prisant, M.G., Videau, L.L., Deis, L.N., Verma, V., Keedy, D.A., Hintze, B.J., Chen, V.B., et al. (2018). MolProbity: More and better reference data for improved all-atom structure validation. Protein Sci. *27*, 293–315. https://doi.org/10.1002/pro.3330.

43. Pettersen, E.F., Goddard, T.D., Huang, C.C., Couch, G.S., Greenblatt, D.M., Meng, E.C., and Ferrin, T.E. (2004). UCSF Chimera–a visualization system for exploratory research and analysis. J. Comput. Chem. *25*, 1605–1612. https://doi.org/10.1002/jcc.20084.

44. Abraham, M.J., Murtola, T., Schulz, R., Páll, S., Smith, J.C., Hess, B., and Lindahl, E. (2015). GROMACS: High performance molecular simulations through multi-level parallelism from laptops to supercomputers. SoftwareX *1–2*, 19–25. https://doi.org/10.1016/j.softx.2015.06.001.

45. Huang, J., and MacKerell, A.D. (2013). CHARMM36 all-atom additive protein force field: validation based on comparison to NMR data. J. Comput. Chem. *34*, 2135–2145. https://doi.org/10.1002/jcc.23354.

46. Vanommeslaeghe, K., Hatcher, E., Acharya, C., Kundu, S., Zhong, S., Shim, J., Darian, E., Guvench, O., Lopes, P., Vorobyov, I., and Mackerell, A.D., Jr. (2010). CHARMM general force field: A force field for drug-like molecules compatible with the CHARMM all-atom additive biological force fields. J. Comput. Chem. *31*, 671–690. https://doi.org/10.1002/jcc.21367.

47. McGibbon, R.T., Beauchamp, K.A., Harrigan, M.P., Klein, C., Swails, J.M., Hernández, C.X., Schwantes, C.R., Wang, L.-P., Lane, T.J., and Pande, V.S. (2015). MDTraj: A Modern Open Library for the Analysis of Molecular Dynamics Trajectories. Biophys. J. *109*, 1528–1532. https://doi.org/10.1016/j.bpj.2015.08.015.

48. Evans, P.R., and Murshudov, G.N. (2013). How good are my data and what is the resolution? Acta Crystallogr. D Biol. Crystallogr. *69*, 1204–1214. https://doi.org/10.1107/S0907444913000061.

49. Vagin, A., and Teplyakov, A. (2010). Molecular replacement with *MOLREP*. Acta Crystallogr. D Biol. Crystallogr. *66*, 22–25. https://doi.org/10.1107/S0907444909042589.

50. Murshudov, G.N., Skubák, P., Lebedev, A.A., Pannu, N.S., Steiner, R.A., Nicholls, R.A., Winn, M.D., Long, F., and Vagin, A.A. (2011). *REFMAC* 5 for the refinement of macromolecular crystal structures. Acta Crystallogr. D Biol. Crystallogr. *67*, 355–367. https://doi.org/10.1107/S0907444911001314.

51. Emsley, P., Lohkamp, B., Scott, W.G., and Cowtan, K. (2010). Features and development of *Coot*. Acta Crystallogr. D Biol. Crystallogr. *66*, 486–501. https://doi.org/10.1107/S0907444910007493.

52. Tickle, I.J., Laskowski, R.A., and Moss, D.S. (1998). R_{free} and the R_{free} Ratio. I. Derivation of Expected Values of Cross-Validation Residuals Used in Macromolecular Least-Squares Refinement. Acta Crystallogr. D Biol. Crystallogr. *54*, 547–557. https://doi.org/10.1107/S0907444997013875.

53. Del Galdo, S., Marracino, P., D'Abramo, M., and Amadei, A. (2015). In silico characterization of protein partial molecular volumes and hydration shells. Phys. Chem. Chem. Phys. *17*, 31270–31277. https://doi.org/10.1039/c5cp05891k.

54. Bussi, G., Donadio, D., and Parrinello, M. (2007). Canonical sampling through velocity rescaling. J. Chem. Phys. *126*, 014101. https://doi.org/10.1063/1.2408420.

55. Darden, T., York, D., and Pedersen, L. (1993). Particle mesh Ewald: An $N \cdot \log(N)$ method for Ewald sums in large systems. J. Chem. Phys. *98*, 10089–10092. https://doi.org/10.1063/1.464397.

56. Essmann, U., Perera, L., Berkowitz, M.L., Darden, T., Lee, H., and Pedersen, L.G. (1995). A smooth particle mesh Ewald method. J. Chem. Phys. *103*, 8577–8593. https://doi.org/10.1063/1.470117.

Please cite this article in press as: Costanzo et al., Binding of steroid substrates reveals the key to the productive transition of the cytochrome P450 OleP, Structure (2024), https://doi.org/10.1016/j.str.2024.06.005

STAR★METHODS

KEY RESOURCES TABLE

REAGENT or RESOURCE	SOURCE	IDENTIFIER
Bacterial and virus strains		
BL21 (DE3) competent cells	Novagen	Cat#69450
Chemicals, peptides, and recombinant proteins		
Lithocholic acid	Merck	Cat#L6250
Testosterone C-IIIN	Merck	Cat#86500
Deposited data		
OleP in complex with testosterone	this study	PDB 8QRD
OleP in complex with lithocholic acid	this study	PDB 8QYI
OleP in complex with 6-deoxyerythronolide B	Parisi et al.[16]	PDB 5MNS
Recombinant DNA		
Plasmid: pET28bOleP	Montemiglio et al.[37]	N/A
Software and algorithms		
Kaleidagraph 4.1.3	Synergy Software	https://www.synergy.com/
Prism 6	GraphPad Software	https://www.graphpad.com/
XDS	Kabsch[38]	https://xds.mr.mpg.de/
CCP4 7.1.016	Dodson et al.[39]	https://www.ccp4.ac.uk/
COOT 0.9.8.8	Emsley and Cowtan[40]	https://www2.mrc-lmb.cam.ac.uk/personal/pemsley/coot/
MolProbity	Chen et al.[41]; Williams et al.[42]	http://molprobity.biochem.duke.edu/
UCSF Chimera	Pattersen et al.[43]	https://www.cgl.ucsf.edu/chimera/download.html
Gromacs 2022	Abraham et al.[44]	https://manual.gromacs.org/2022/download.html
CHARMM36	Huang et al.[45]; Vanommeslaeghe et al.[46]	https://www.charmm.org/archive/charmm/resources/charmm-force-fields/
MdTraj	McGibbon et al.[47]	https://www.mdtraj.org/1.9.8.dev0/index.html

RESOURCE AVAILABILITY

Lead contact

Further information and requests for resources or reagents should be directed to and will be fulfilled by the lead contact, Dr. Linda Celeste Montemiglio (lindaceleste.montemiglio@cnr.it).

Materials availability

This study did not generate new unique reagents.

Data and code availability

The structural data (atomic coordinates and structural factors) have been deposited in the Protein DataBank (https://www.rcsb.org) and are publicly available as of the date of publication. Accession numbers are listed in the key resources table. This paper does not report original code. Any additional information required to reanalyze the data reported in this paper is available from the lead contact upon request.

EXPERIMENTAL MODEL AND STUDY PARTICIPANT DETAILS

Bacterial strains

All proteins used for biochemical studies were recombinantly expressed in Escherichia coli BL21 (DE3) strain (Novagen, 69450).

Please cite this article in press as: Costanzo et al., Binding of steroid substrates reveals the key to the productive transition of the cytochrome P450 OleP, Structure (2024), https://doi.org/10.1016/j.str.2024.06.005

METHOD DETAILS

OleP expression and purification

The gene of OleP (Uniprot: Q59819) was cloned into a pET28b(+) vector using NdeI/BglII restriction sites. The resulting protein contained a hexahistidine tag at its N-terminus followed by thrombin cleavage site. The protein was expressed in Escherichia coli BL21 (DE3) cells and purified as previously described.[37] In brief, transformed E. coli BL21 (DE3) cells were grown for about 70 h at 293 K in Luria Broth medium, containing kanamycin resistance and 1.5 mM of the heme precursor δ-aminolevulinic acid (δ-ALA). The bacteria were harvested by centrifugation and resuspended in lysis buffer (50 mM Tris·HCl and 300 mM NaCl, pH 8.0) and lysed by addition of a mixture of deoxyribonuclease, ribonuclease, lysozyme (Sigma Aldrich, St. Louise, Missouri, USA), protease inhibitors (cOmplete, EDTA-free, Roche, Basel, Switzerland), followed by sonication. The soluble fraction of the lysate was immobilized on a 5 mL Hi-Trap Chelating HP column (GE Healthcare, Buckinghamshire, UK) equilibrated with lysis buffer. OleP was eluted using lysis buffer supplemented with 200 mM imidazole. The His-tag was digested using bovine thrombin protease (Sigma Aldrich, St. Louise, Missouri, USA) at 277 K overnight (∼16 h) and removed by a reverse passage into 5 mL Hi-Trap Chelating HP column. The protein was further purified by ion-exchange chromatography using a Mono Q colum (GE Healthcare) in 20 mM Bis-Tris, pH 6.0, using increasing concentration of NaCl. OleP elutes around 0.1 M NaCl.

Sample homogeneity and monodispersion were evaluated by SDS-PAGE and gel filtration chromatography using a 10/400 column packed with Tosoh HW-55S (Tosoh Bioscience) resin in a buffer containing 20 mM Tris·HCl and 200 mM NaCl, pH 8.0. Under these conditions, OleP elutes as a monomer.[37]

Crystallization of OleP in complex with TES and LCA

To obtain OleP crystals in complex with TES and LCA, the purified protein was concentrated to a final concentration of 19 mg/mL (0.45 mM) in 20 mM Tris·HCl and 200 mM NaCl, pH 8.0, and co-crystallized in the presence of saturating concentrations of the ligand, namely 1 mM TES and 1 mM LCA, by the hanging drop vapor diffusion technique at 295 K. Each protein-ligand complex was mixed in a 1:1 ratio with the reservoir solution and equilibrated against 500 μL of the reservoir solution. Diffracting crystals of the complexes were grown in 4.4 M sodium formate. The quality of the X-ray diffraction data was improved by performing a streak seeding for both protein-ligand complexes. Crystals were flash-frozen in liquid nitrogen without prior additional cryo-protection.

Equilibrium binding analysis

The binding affinity to TES and LCA was determined at 298 K by titrating OleP at a concentration between 1.5 and 2 μM in a total volume of 750 μL of 50 mM HEPES and 200 mM NaCl, pH 7.5. Dimethyl sulfoxide (DMSO) was used to prepare the stock solutions of the ligands. DMSO, TES, and LCA were purchased from Merck Millipore (Burlington, MA, USA). After each addition, a waiting time of approximately 2 min was observed.

The final concentrations of TES and LCA ranged from 0 to 200 μM and from 0 to 50 μM, respectively, in compliance with the relative ligand solubility. The final percentage of DMSO did not exceed 1% (v/v). The appropriate blank was subtracted, and UV-visible spectra (200–700 nm) were recorded after each ligand addition using a Jasco V-650 spectrophotometer equipped with a Jasco programmable Peltier element (EHC-716) to ensure a controlled temperature. Ligand binding was monitored by following the typical type I absorption shift of the heme γ-Soret peak of OleP, from 417 to 380–390 nm. The absorbance intensities at 417 nm and 388 nm were plotted against ligand concentration.

To monitor the effect of the ionic strength on the spin-state equilibrium in OleP bound to steroids, 2 μM protein in the presence of 50 μM of LCA and 200 μM of TES was titrated at 298 K with an increasing concentration of sodium formate, ranging from 0 to 3.5 M, in a final volume of 750 μL of 50 mM HEPES and 200 mM NaCl, pH 7.5. The absorption shift of the Soret peak was followed by collecting UV-visible spectra (200–800 nm) after each substrate addition, and the appropriate blank was subtracted.

X-Ray data collection and analysis

X-ray diffraction data were collected at 100 K on a PILATUS detector (Dectris, Baden-Dättwil, Switzerland) at ELETTRA synchrotron (beamline XRD2, Trieste, Italy) and processed by means of the XDS package[38] and Aimless.[48] The crystallization conditions, data collection, and the statistics of the refinement are reported in Table S2.

Structure determination and refinement

The initial phases were calculated by molecular replacement using the program MOLREP of the CCP4 suite.[49]

The resulting models were reconstructed starting from the coordinates of a single closed monomer OleP in complex with 6DEB obtained in high salt conditions (PDB 5MNS,[16]) deprived of ligands, waters and ions, and used as search model. Six monomers (A–F) were found in the asymmetric unit of both structures. Model building and refinement were performed with Refmac5 in the CCP4 suite[39,50] and Coot 0.9.8.8,[40,51] using the |Fo|–|Fc| map contoured at ± 3 σ and the 2|Fo|–|Fc| at ± 1 σ. Five percent of the reflections were excluded from refinement and used for the R free calculation.[52] The resulting structures were refined using automatic weighting with isotropic B-factors and TLS, considering one TLS group per protein chain. Water molecules were added both automatically and manually using COOT.

In the two structures, the first 10 to 13 residues at the N-terminus are missing because of the poor electron density contouring the region, which is caused by the intrinsic structural flexibility of the N-terminal tail. In addition, in both structures the F monomer has a weak electron density if compared to the other copies.

The geometric quality of the final models was assessed with MolProbity.[41,42] All figures were produced using UCSF Chimera.[43] The atomic coordinates and structure factors of TES-OleP and LCA-OleP have been deposited in the Protein DataBank (accession numbers PDB 8QRD and PDB 8QYI, respectively).

Molecular dynamics simulations

All-atoms Molecular Dynamics (MD) simulations were performed on monomer C of the TES-OleP and LCA-OleP complexes using Gromacs 2022 software package.[44] CHARMM36 was used as forcefield while the missing parameters of TES were obtained through CGenFF.[45,46] For both systems, the simulations were conducted using the same procedure described hereafter. The complex was centered in a cubic box, large enough to avoid boundary effects, and then solvated with TIP3P water model and neutralizing ions (Na^+). After a minimization step, using the steepest descent algorithm, the system was equilibrated in the NVT ensemble, by performing a series of short runs (each lasting 50 ps), during which the box dimensions were adjusted to correctly reproduce the experimental water density.[53] Thereafter, the production runs (two replicas of about 600 ns for each system) were started in the same ensemble.

For both equilibration and production steps, the temperature was kept constant at 300 K using the velocity rescale algorithm,[54] the integration timestep was set at 2 fs, and the electrostatic interactions were calculated according to the Particle Mesh Ewald (PME) method,[55,56] using a 1.2 nm cut-off. The same cut-off value was used for the van der Waals interactions.

The stability of the binding pose, as obtained by the crystallographic structure, was evaluated by calculating: i) the Euclidean distances between the Fe atom of the heme group and the ligand carbon atoms that can be hydroxylated; ii) the average distances between the ligand and the surrounding residues, defined by a sphere of 8 Å centered in center of mass of the ligand; iii) the hydrogen bonds that the ligand establishes with the OleP active site. Such calculations were performed for both replicates, using either Gromacs or MdTraj tools.[47]

QUANTIFICATION AND STATISTICAL ANALYSIS

Equilibrium binding data analysis

The dissociation constant, K_D, was determined using the Kaleidagraph software package. Non-linear regression analysis was performed by means of the hyperbolic equation:

$$\Delta AU_{obs} = \Delta AU_{max}[L] / (K_D + [L]),$$

where ΔAU_{obs} is the difference in absorbance, ΔAU_{max} is the maximum difference in absorbance extrapolated to infinite ligand concentration, and [L] is the analytical concentration of the ligand. All data were globally fitted using Prism 6 software (GraphPad). The percentage of high spin content was determined following the Jung's procedure.[22] All reported values are mean ± SD for three independent experiments.

Crystallographic data collection and processing

Crystallographic data collection and refinement statistics are shown in Table S2.